PHYSICAL REVIEW D **88,** 052015 (2013)

Studies of the decays $B^+ \to p\bar{p}h^+$ and observation of $B^+ \to \bar{\Lambda}(1520)p$

R. Aaij *et al.**
(LHCb Collaboration)

(Received 23 July 2013; published 19 September 2013)

Dynamics and direct CP violation in three-body charmless decays of charged B mesons to a proton, an antiproton and a light meson (pion or kaon) are studied using data, corresponding to an integrated luminosity of 1.0 fb^{-1}, collected by the LHCb experiment in pp collisions at a center-of-mass energy of 7 TeV. Production spectra are determined as a function of Dalitz-plot and helicity variables. The forward-backward asymmetry of the light meson in the $p\bar{p}$ rest frame is measured. No significant CP asymmetry in $B^+ \to p\bar{p}K^+$ decay is found in any region of the Dalitz plane. We present the first observation of the decay $B^+ \to \bar{\Lambda}(1520)(\to K^+\bar{p})p$ near the $K^+\bar{p}$ threshold and measure $\mathcal{B}(B^+ \to \bar{\Lambda}(1520)p) = (3.9^{+1.0}_{-0.9}(\text{stat}) \pm 0.1(\text{syst}) \pm 0.3(\text{BF})) \times 10^{-7}$, where BF denotes the uncertainty on secondary branching fractions.

DOI: 10.1103/PhysRevD.88.052015 PACS numbers: 13.25.Hw

I. INTRODUCTION

Evidence of inclusive direct CP violation in three-body charmless decays of B^+ mesons[1] has recently been found in the modes $B^+ \to K^+\pi^+\pi^-$, $B^+ \to K^+K^+K^-$, $B^+ \to \pi^+\pi^+\pi^-$, and $B^+ \to K^+K^-\pi^+$ [1,2]. In addition, very large CP asymmetries were observed in the low K^+K^- and $\pi^+\pi^-$ mass regions, without clear connection to a resonance. The localization of the asymmetries and the correlation of the CP violation between the decays suggest that $\pi^+\pi^- \leftrightarrow K^+K^-$ rescattering may play an important role in the generation of the strong phase difference needed for such a violation to occur [3,4]. Conservation of CPT symmetry imposes a constraint on the sum of the rates of final states with the same flavor quantum numbers, providing the possibility of entangled long-range effects contributing to the CP violating mechanism [5]. In contrast, $h^+h^- \leftrightarrow p\bar{p}$ ($h = \pi$ or K throughout the paper) rescattering is expected to be suppressed compared to $\pi^+\pi^- \leftrightarrow K^+K^-$, and thus is not expected to play an important role.

The leading quark-level diagrams for the modes $B^+ \to p\bar{p}h^+$ are shown in Fig. 1. The $B^+ \to p\bar{p}K^+$ mode is expected to be dominated by the $b \to s$ loop (penguin) transition while the mode $B^+ \to p\bar{p}p\pi^+$ is likely to be dominated by the $b \to u$ tree decay, which is Cabibbo-Kobayashi-Maskawa matrix suppressed compared to the former. Since the short distance dynamics are similar to that of the $B^+ \to h^+h^+h^-$ modes, a CP analysis of $B^+ \to p\bar{p}h^+$ decays could help to clarify the role of long-range scatterings in the CP asymmetries of $B^+ \to h^+h^+h^-$ decays.

First studies were performed at the B factories on the production and dynamics of $B^+ \to p\bar{p}h^+$ decays [6–8]. The results have shown a puzzling opposite behavior of $B^+ \to p\bar{p}K^+$ and $B^+ \to p\bar{p}\pi^+$ decays in the asymmetric occupation of the Dalitz plane. Charmonium contributions to the $B^+ \to p\bar{p}K^+$ decay have been studied by LHCb [9]. This paper reports a detailed study of the dynamics of the $B^+ \to p\bar{p}h^+$ decays and a systematic search for CP violation, both inclusively and in regions of the Dalitz plane. The charmless region, defined for the invariant mass $m_{p\bar{p}} < 2.85$ GeV$/c^2$, is of particular interest. The relevant observables are the differential production spectra of Dalitz-plot variables and the global charge asymmetry A_{CP}, defined as

$$A_{CP} = \frac{N(B^- \to f^-) - N(B^+ \to f^+)}{N(B^- \to f^-) + N(B^+ \to f^+)}, \tag{1}$$

where $f^\pm = p\bar{p}h^\pm$. The mode $B^+ \to J/\psi(\to p\bar{p})K^+$ serves as a control channel. The first observation of the decay $B^+ \to \bar{\Lambda}(1520)p$ is presented. Its branching fraction is derived through the ratio of its yield to the measured yield of the $B^+ \to J/\psi(\to p\bar{p})K^+$ decay.

II. DETECTOR AND SOFTWARE

The LHCb detector [10] is a single-arm forward spectrometer covering the pseudorapidity range $2 < \eta < 5$, designed for the study of particles containing b or c quarks. The detector includes a high precision tracking system consisting of a silicon-strip vertex detector surrounding the pp interaction region, a large-area silicon-strip detector located upstream of a dipole magnet with a bending power of about 4 Tm, and three stations of silicon-strip detectors and straw drift tubes placed downstream. The combined tracking system has momentum resolution $\Delta p/p$ that varies from 0.4% at 5 GeV$/c$ to 0.6% at 100 GeV$/c$, and

*Full author list given at the end of the article.

[1]Throughout the paper, the inclusion of charge conjugate processes is implied, except in the definition of CP asymmetries.

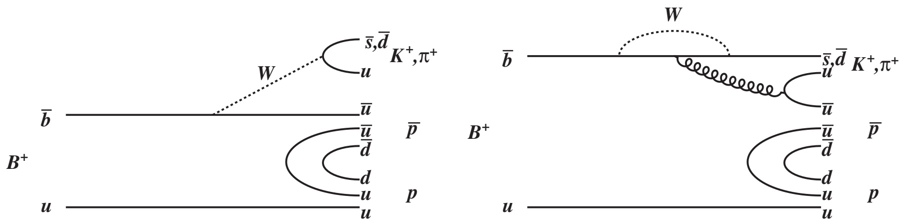

FIG. 1. Leading tree and penguin diagrams for $B^+ \to p\bar{p}h^+$ decays.

impact parameter (IP) resolution of 20 μm for tracks with high transverse momentum. Charged hadrons are identified using two ring-imaging Cherenkov detectors (RICH) [11]. Photon, electron and hadron candidates are identified by a calorimeter system consisting of scintillating-pad and preshower detectors, an electromagnetic calorimeter and a hadronic calorimeter. Muons are identified by a system composed of alternating layers of iron and multiwire proportional chambers.

The trigger [12] consists of a hardware stage, based on information from the calorimeter and muon systems, followed by a software stage which applies a full event reconstruction. Events triggered both on objects independent of the signal, and associated with the signal, are used. In the latter case, the transverse energy of the hadronic cluster is required to be at least 3.5 GeV. The software trigger requires a two-, three- or four-track secondary vertex with a large sum of the transverse momentum, $p_{\rm T}$, of the tracks and a significant displacement from all primary pp interaction vertices. At least one track must have $p_{\rm T} > 1.7$ GeV$/c$, track fit χ^2 per degree of freedom less than 2, and an impact parameter χ^2 ($\chi^2_{\rm IP}$) with respect to any primary interaction greater than 16. The $\chi^2_{\rm IP}$ is defined as the difference between the χ^2 of the primary vertex reconstructed with and without the considered track. A multivariate algorithm is used to identify secondary vertices [13].

The simulated pp collisions are generated using PYTHIA 6.4 [14] with a specific LHCb configuration [15]. Decays of hadronic particles are described by EVTGEN [16] in which final state radiation is generated using PHOTOS [17]. The interaction of the generated particles with the detector and its response are implemented using the GEANT4 toolkit [18] as described in Ref. [19]. Nonresonant $B^+ \to p\bar{p}h^+$ events are simulated, uniformly distributed in phase space, to study the variation of efficiencies across the Dalitz plane, as well as resonant samples such as $B^+ \to J/\psi(\to p\bar{p})K^+$, $B^+ \to \eta_c(\to p\bar{p})K^+$, $B^+ \to \psi(2S)(\to p\bar{p})K^+$, $B^+ \to \bar{\Lambda}(1520)(\to K^+\bar{p})p$, and $B^+ \to J/\psi(\to p\bar{p})\pi^+$.

III. SIGNAL RECONSTRUCTION AND DETERMINATION

Candidate $B^+ \to p\bar{p}h^+$ decays are formed by combining three charged tracks, with appropriate mass assignments. The tracks are required to satisfy track fit quality criteria and a set of loose selection requirements on their momenta, transverse momenta, $\chi^2_{\rm IP}$, and distance of closest approach between any pair of tracks. The requirement on the momentum of the proton candidates, $p > 3$ GeV$/c$, is larger than for the kaon and pion candidates, $p > 1.5$ GeV$/c$. The B^+ candidates formed by the combinations are required to have $p_{\rm T} > 1.7$ GeV$/c$ and $\chi^2_{\rm IP} < 10$. The distance between the decay vertex and the primary vertex is required to be greater than 3 mm, and the vector formed by the primary and decay vertices must align with the B^+ candidate momentum. Particle identification (PID) is applied to the proton, kaon and pion candidates, using combined subdetector information, the main separation power being provided by the RICH system. The PID efficiencies are derived from data calibration samples of kinematically identified pions, kaons and protons originating from the decays $D^{*+} \to D^0(\to K^-\pi^+)\pi^+$ and $\Lambda \to p\pi^-$.

Signal and background are extracted using unbinned extended maximum likelihood fits to the mass of the $p\bar{p}h^+$ combinations. The $B^+ \to p\bar{p}K^+$ signal is modeled by a double Gaussian function. The combinatorial background is represented by a second-order polynomial function. A Gaussian function accounting for a partially reconstructed component from $B \to p\bar{p}K^*$ decays is used. A possible $p\bar{p}\pi^+$ cross-feed contribution is included in the fit and is found to be small. An asymmetric Gaussian function with power law tails is used to estimate the uncertainties related to the variation of the signal yield.

In the case of the $B^+ \to p\bar{p}\pi^+$ decay, the signal yield is smaller and the background is larger. The ranges of the signal and cross-feed parameters are constrained to the values obtained in the simulation within their uncertainties. The signal and the $p\bar{p}K^+$ cross-feed contribution are modeled with Gaussian functions. The combinatorial background is represented by a third-order polynomial function.

The $B^+ \to p\bar{p}h^+$ invariant mass spectra are shown in Fig. 2. The signal yields obtained from the fits are $N(p\bar{p}K^\pm) = 7029 \pm 139$ and $N(p\bar{p}\pi^\pm) = 656 \pm 70$, where the uncertainties are statistical only.

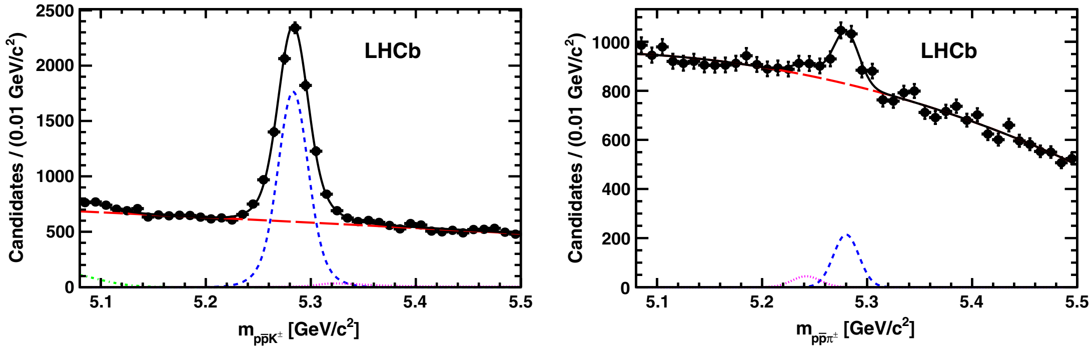

FIG. 2 (color online). Invariant mass distributions of (left) $p\bar{p}K^+$ and (right) $p\bar{p}\pi^+$ candidates. The points with error bars represent data. The solid black line represents the total fit function. Blue dashed, purple dotted, red long-dashed and green dashed-dotted curves represent the signal, cross-feed, combinatorial background and partially reconstructed background, respectively.

IV. DYNAMICS OF $B^+ \to p\bar{p}h^+$ DECAYS

To probe the dynamics of the $B^+ \to p\bar{p}h^+$ decays, differential production spectra are derived as a function of $m_{p\bar{p}}$ and $\cos\theta_p$, where θ_p is the angle between the charged meson h and the opposite-sign baryon in the rest frame of the $p\bar{p}$ system. The $p\bar{p}h^+$ invariant mass is fitted in bins of the aforementioned variables and the signal yields are corrected for trigger, reconstruction and selection efficiencies. They are estimated with simulated samples and corrected to account for discrepancies between data and simulation. The signal yields are determined with the fit models described in the previous section, but allowing the combinatorial background parameters to vary. The systematic uncertainties are determined for each bin and include uncertainties related to the PID correction, fit model, trigger efficiency, and the size of the simulated samples. The latter is evaluated from the differences between data and simulation as a function of the Dalitz-plot variables. No trigger-induced distortions are found.

TABLE I. Fitted $B^+ \to p\bar{p}K^+$ signal yield, including the charmonium modes, efficiency and relative systematic uncertainty, in bins of $p\bar{p}$ invariant mass. The error on the efficiency includes all the sources of uncertainty.

$m_{p\bar{p}}$ [GeV/c^2]	$B^+ \to p\bar{p}K^+$ yield	Efficiency (%)	Systematics (%)
<2.85	3315 ± 83	1.74 ± 0.04	2.9
<2	446 ± 32	1.80 ± 0.08	8.1
[2, 2.2]	1001 ± 42	1.77 ± 0.05	4.4
[2.2, 2.4]	732 ± 39	1.77 ± 0.03	4.0
[2.4, 2.6]	550 ± 35	1.67 ± 0.03	3.4
[2.6, 2.85]	580 ± 34	1.67 ± 0.02	2.9
[2.85, 3.15]	2768 ± 58	1.61 ± 0.02	2.6
[3.15, 3.3]	125 ± 18	1.57 ± 0.03	3.8
[3.3, 4]	585 ± 37	1.47 ± 0.01	2.2
>4	233 ± 32	1.22 ± 0.01	2.3

A. Invariant mass of the $p\bar{p}$ system

The yields and total efficiency for $B^+ \to p\bar{p}h^+$ in $m_{p\bar{p}}$ bins are shown in Tables I and II. The charmonium contributions originate from the decays $B^+ \to J/\psi(\to p\bar{p})K^+$, $B^+ \to \eta_c(\to p\bar{p})K^+$ and $B^+ \to \psi(2S)(\to p\bar{p})K^+$ for the $B^+ \to p\bar{p}K^+$ mode, and $B^+ \to J/\psi(\to p\bar{p})\pi^+$ for the $B^+ \to p\bar{p}\pi^+$ mode. Before deriving the distributions, the charmonium contributions are unfolded by

TABLE II. Fitted $B^+ \to p\bar{p}\pi^+$ signal yield, including the J/ψ mode, $B^+ \to p\bar{p}K^+$ cross-feed yield, signal efficiency, and relative systematic uncertainty in bins of $p\bar{p}$ invariant mass.

$m_{p\bar{p}}$ [GeV/c^2]	$B^+ \to p\bar{p}\pi^+$ yield	$B^+ \to p\bar{p}K^+$ cross-feed	Efficiency (%)	Systematics (%)
<2.85	564 ± 61	114 ± 62	1.31 ± 0.10	7.6
<2	140 ± 26	64 ± 26	1.34 ± 0.15	11
[2, 2.2]	261 ± 31	10 ± 29	1.30 ± 0.10	7.9
[2.2, 2.4]	95 ± 30	0 ± 39	1.33 ± 0.09	7.1
[2.4, 2.6]	48 ± 28	14 ± 30	1.35 ± 0.09	6.4
[2.6, 2.85]	21 ± 20	35 ± 23	1.26 ± 0.07	5.9
[2.85, 3.15]	72 ± 19	12 ± 18	1.28 ± 0.07	5.5
[3.15, 3.3]	19 ± 11	0 ± 3	1.24 ± 0.08	6.7
[3.3, 4]	0 ± 7	0 ± 23	1.24 ± 0.06	4.7
>4	23 ± 21	57 ± 23	0.94 ± 0.05	4.9

TABLE III. Yields, efficiencies and relative systematic uncertainties of the charmonium modes from the combined $(m_{p\bar{p}h^+}, m_{p\bar{p}})$ fits for the regions $m_{p\bar{p}} \in [2.85, 3.15]$ GeV$/c^2$ (for both $B^+ \to p\bar{p}K^+$ and $B^+ \to p\bar{p}\pi^+$) and $[3.60, 3.75]$ GeV$/c^2$ (for $B^+ \to p\bar{p}K^+$).

Mode	Yield	Efficiency (%)	Systematics (%)
$B^+ \to J/\psi(\to p\bar{p})K^+$	1413 ± 40	1.624 ± 0.005	1.8
$B^+ \to \eta_c(\to p\bar{p})K^+$	722 ± 36	1.660 ± 0.005	2.0
$B^+ \to \psi(2S)(\to p\bar{p})K^+$	132 ± 16	1.475 ± 0.011	1.5
$B^+ \to J/\psi(\to p\bar{p})\pi^+$	59 ± 11	1.328 ± 0.011	4.2

performing two dimensional extended unbinned maximum likelihood fits to the $p\bar{p}h^+$ and $p\bar{p}$ invariant masses. The J/ψ and $\psi(2S)$ resonances are modeled by Gaussian functions and the η_c resonance is modeled by a convolution of Breit-Wigner and Gaussian functions. The nonresonant $p\bar{p}$ component and the combinatorial background are modeled by polynomial shapes. Table III shows the yields of contributing charmonium modes. The results are consistent with those reported in Ref. [9].

After unfolding, the efficiency-corrected differential distributions are shown in Fig. 3. An enhancement is observed at low $p\bar{p}$ mass both for $B^+ \to p\bar{p}K^+$ and $B^+ \to p\bar{p}\pi^+$, with a more sharply peaked distribution for $B^+ \to p\bar{p}\pi^+$. This accumulation of events at low $m_{p\bar{p}}$ is a well known feature that has also been observed in different contexts such as $\Upsilon(1S) \to \gamma p\bar{p}$ [20], $J/\psi \to \gamma p\bar{p}$ [21] and $B^0 \to D^{(*)0} p\bar{p}$ [22] decays. It appears to be caused by proton-antiproton rescattering and is modulated by the particular kinematics of the decay from which the $p\bar{p}$ pair originates [23].

B. Invariant mass squared of the Kp system

The $B^+ \to p\bar{p}K^+$ signal yield as a function of the Dalitz-plot variable m^2_{Kp} is considered, where Kp denotes the neutral combinations K^-p or $K^+\bar{p}$. Table IV shows the yields and efficiencies, after the charmonium bands have been vetoed in the ranges $m_{p\bar{p}} \in [2.85, 3.15]$ GeV$/c^2$ and $[3.60, 3.75]$ GeV$/c^2$. The differential spectrum derived after efficiency correction is shown in Fig. 4. Contrary to the situation for $m_{p\bar{p}}$, the data distribution is in reasonable agreement with the uniform phase space distribution, with some discrepancies in the region $m^2_{Kp} \in [4, 12]$ (GeV$/c^2)^2$.

TABLE IV. Fitted $B^+ \to p\bar{p}K^+$ yields after subtracting the charmonium bands, efficiencies and relative systematic uncertainties in bins of Kp invariant mass squared.

m^2_{Kp} [(GeV$/c^2)^2$]	$B^+ \to p\bar{p}K^+$ yield	Efficiency (%)	Systematics (%)
<4	454 ± 37	1.40 ± 0.02	3.3
[4, 6]	522 ± 36	1.43 ± 0.02	2.5
[6, 8]	797 ± 37	1.45 ± 0.01	2.6
[8, 10]	702 ± 42	1.51 ± 0.01	2.6
[10, 12]	445 ± 32	1.53 ± 0.01	2.8
[12, 14]	526 ± 34	1.66 ± 0.01	2.8
[14, 16]	338 ± 29	1.67 ± 0.02	3.4
>16	305 ± 28	1.66 ± 0.02	3.5

C. Helicity angle of the $p\bar{p}$ system

The $B^+ \to p\bar{p}h^+$ signal yields are considered as a function of $\cos\theta_p$. Tables V and VI show the corresponding yields and efficiencies. The differential distributions are shown in Fig. 5.

The forward-backward asymmetries are derived by comparing the yields for $\cos\theta_p > 0$ and $\cos\theta_p < 0$, accounting for the weighted-average efficiencies in each region

$$A_{\rm FB} = \frac{\frac{N_{\rm pos}}{\epsilon_{\rm pos}} - \frac{N_{\rm neg}}{\epsilon_{\rm neg}}}{\frac{N_{\rm pos}}{\epsilon_{\rm pos}} + \frac{N_{\rm neg}}{\epsilon_{\rm neg}}} = \frac{N_{\rm pos} - fN_{\rm neg}}{N_{\rm pos} + fN_{\rm neg}}, \quad (2)$$

where $\epsilon_{\rm pos} = \epsilon(\cos\theta_p > 0)$ and $\epsilon_{\rm neg} = \epsilon(\cos\theta_p < 0)$ are the averaged efficiencies, $f = \epsilon_{\rm pos}/\epsilon_{\rm neg}$ and

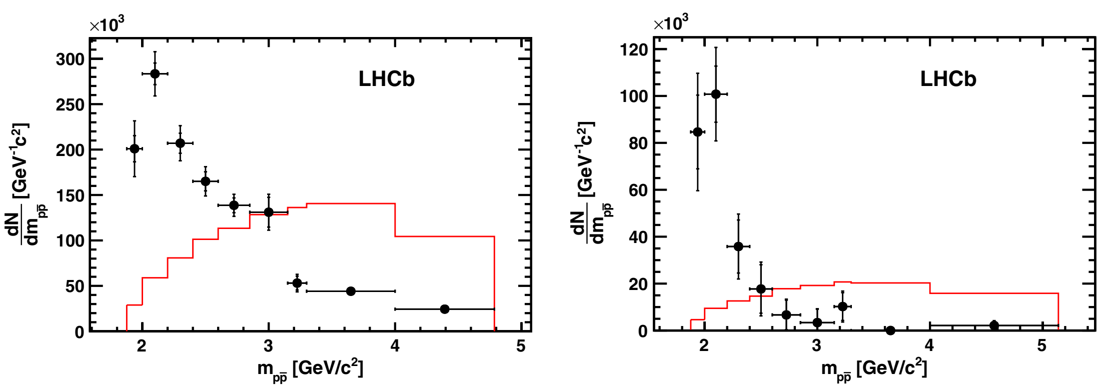

FIG. 3 (color online). Efficiency-corrected differential yield as a function of $m_{p\bar{p}}$ for (left) $B^+ \to p\bar{p}K^+$ and (right) $B^+ \to p\bar{p}\pi^+$. The data points are shown with their statistical and total uncertainties. For comparison, the solid lines represent the expectations for a uniform phase space production, normalized to the efficiency-corrected area.

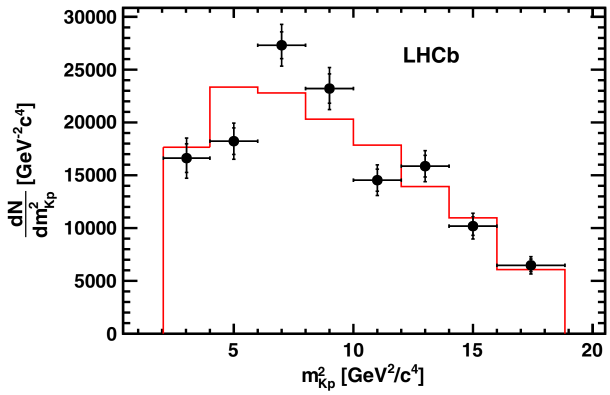

FIG. 4 (color online). Efficiency-corrected differential yield as a function of m^2_{Kp} for $B^+ \to p\bar{p}K^+$. The data points are shown with their statistical and total uncertainties. The solid line represents the expectation for a uniform phase space production, normalized to the efficiency-corrected area, for comparison.

$N_{\rm pos} = N(\cos\theta_p > 0)$, $N_{\rm neg} = N(\cos\theta_p < 0)$. The values obtained are $A_{\rm FB}(p\bar{p}K^+) = 0.370 \pm 0.018({\rm stat}) \pm 0.016({\rm syst})$ and $A_{\rm FB}(p\bar{p}\pi^+) = -0.392 \pm 0.117({\rm stat}) \pm 0.015({\rm syst})$, where the systematic uncertainties are evaluated from the uncertainties on the efficiencies listed in Tables V and VI, taking into account the relative weights of the bins.

A clear opposite angular correlation between $B^+ \to p\bar{p}K^+$ and $B^+ \to p\bar{p}\pi^+$ decays is observed; the light meson h tends to align with the opposite-sign baryon for $B^\pm \to p\bar{p}K^\pm$ while it aligns with the same-sign baryon for the $B^\pm \to p\bar{p}\pi^\pm$ mode. A quark level analysis suggests that the meson should align with the same-sign baryon, since the opposite-sign baryon has larger momentum, being formed by products from the decaying quark [24]. This is in agreement with the angular spectrum of $B^+ \to p\bar{p}\pi^+$ but not for $B^+ \to p\bar{p}K^+$ decays.

D. Dalitz plot

From the fits to the B-candidate invariant mass, shown in Fig. 2, signal weights are calculated with the *sPlot* technique [25] and are used to produce the signal Dalitz-plot distributions shown in Fig. 6. To ease the comparison, the $\cos\theta_p$ curves corresponding to the boundaries of the eight bins used to make the angular distributions in Fig. 5 are superimposed.

With the exception of the charmonium bands [η_c, J/ψ, $\psi(2S)$ for $B^+ \to p\bar{p}K^+$, and J/ψ for $B^+ \to p\bar{p}\pi^+$], the structure of the low $p\bar{p}$ mass enhancement is very different between $B^+ \to p\bar{p}K^+$ and $B^+ \to p\bar{p}\pi^+$. The $B^+ \to p\bar{p}K^+$ events are distributed in the middle and lower m^2_{Kp} half, exhibiting a possible $p\bar{p}$ band structure near 4 GeV$^2/c^4$. An enhancement at low m_{Kp} is also observed and is caused to a large extent by a $\Lambda(1520)$ signal, as will be shown in the next section. The $B^+ \to p\bar{p}\pi^+$ events are mainly clustered in the upper $m^2_{\pi p}$ half, with also a few events

TABLE V. Fitted $B^+ \to p\bar{p}K^+$ yields, efficiencies and relative systematic uncertainties in bins of $\cos\theta_p$.

$\cos\theta_p$ range	$B^+ \to p\bar{p}K^+$ yield	Efficiency (%)	Systematics (%)
[−1, −0.75]	508 ± 34	1.54 ± 0.01	2.7
[−0.75, −0.5]	497 ± 31	1.51 ± 0.02	3.0
[−0.5, −0.25]	309 ± 27	1.48 ± 0.01	2.9
[−0.25, 0]	381 ± 28	1.49 ± 0.01	2.6
[0, 0.25]	640 ± 46	1.51 ± 0.01	2.9
[0.25, 0.5]	799 ± 42	1.52 ± 0.01	2.2
[0.5, 0.75]	976 ± 41	1.56 ± 0.01	2.8
[0.75, 1]	1346 ± 51	1.55 ± 0.01	2.7

TABLE VI. Fitted $B^+ \to p\bar{p}\pi^+$ signal yields, efficiencies and relative systematic uncertainties in bins of $\cos\theta_p$.

$\cos\theta_p$ range	$B^+ \to p\bar{p}\pi^+$ yield	Efficiency(%)	Systematics (%)
[−1, −0.75]	150 ± 31	1.23 ± 0.02	5.5
[−0.75, −0.5]	85 ± 27	1.15 ± 0.02	5.5
[−0.5, −0.25]	104 ± 24	1.19 ± 0.02	5.5
[−0.25, 0]	77 ± 23	1.19 ± 0.02	5.5
[0, 0.25]	43 ± 21	1.14 ± 0.02	5.5
[0.25, 0.5]	24 ± 20	1.16 ± 0.02	5.5
[0.5, 0.75]	10 ± 12	1.19 ± 0.02	5.5
[0.75, 1]	93 ± 26	1.19 ± 0.02	5.2

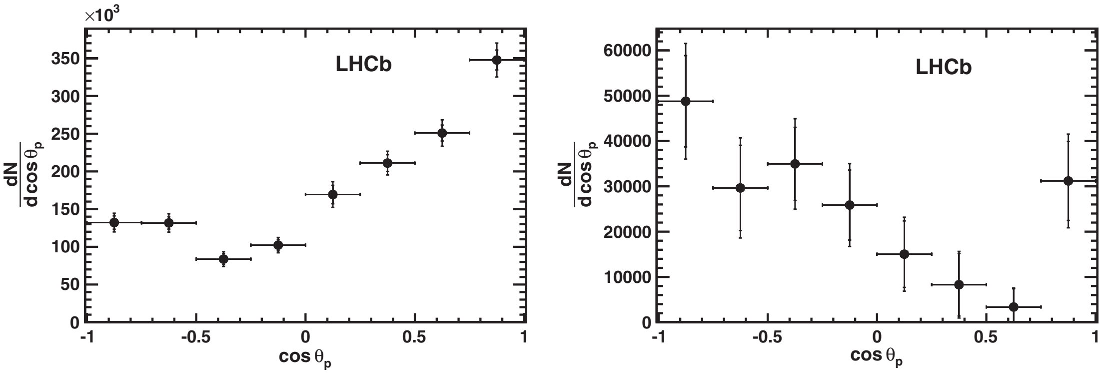

FIG. 5. Efficiency-corrected differential yields as functions of $\cos\theta_p$ for (left) $B^+ \to p\bar{p}K^+$ and (right) $B^+ \to p\bar{p}\pi^+$ modes, after subtraction of the charmonium contributions. The data points are shown with their statistical and total uncertainties.

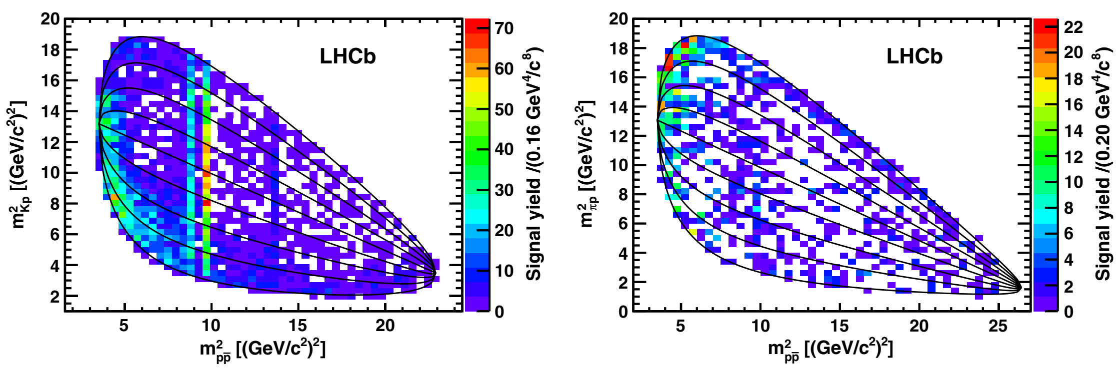

FIG. 6 (color online). Signal weighted Dalitz-plot distributions for (left) $B^+ \to p\bar{p}K^+$ and (right) $B^+ \to p\bar{p}\pi^+$. Also shown are the iso- $\cos\theta_p$ lines corresponding to the $\cos\theta_p$ bin boundaries; $\cos\theta_p = -1$ $(+1)$ is the uppermost (lowermost) line. The distributions are not corrected for efficiency.

on the doubly charged top diagonal $(p\pi)^{++}$ (near the $\cos\theta_p = -1$ boundary). These distributions of events are consistent with the angular distributions and asymmetries reported earlier.

V. MEASUREMENT OF A_{CP} FOR $B^+ \to p\bar{p}K^+$ DECAYS

The raw charge asymmetry is obtained by performing a simultaneous extended unbinned maximum likelihood fit to the B^- and B^+ samples. The $B^\pm$ yields are defined as a function of the total yield N and the raw asymmetry, $A_{\rm raw}$, by $N^\mp = N(1 \pm A_{\rm raw})/2$.

The CP asymmetry is then derived after correcting for the $B^\pm$ production asymmetry $A_{\rm P}(B^\pm)$ and the kaon detection asymmetry $A_{\rm D}(K^\pm)$

$$A_{CP} = A_{\rm raw} - A_{\rm P}(B^\pm) - A_{\rm D}(K^\pm). \quad (3)$$

The correction $A_\Delta = A_{\rm P}(B^\pm) + A_{\rm D}(K^\pm)$ is measured from data with the decay $B^\pm \to J/\psi(\to p\bar{p})K^\pm$ which is part of the data sample

$$A_\Delta = A_{\rm raw}(J/\psi(\to p\bar{p})K^\pm) - A_{CP}(J/\psi K^\pm), \quad (4)$$

where $A_{CP}(J/\psi K^\pm) = (1 \pm 7) \times 10^{-3}$ [26].

Another correction has been applied to account for the proton-antiproton asymmetry, which exactly cancels for $J/\psi(\to p\bar{p})K^\pm$ but not necessarily in the full phase space of $p\bar{p}K^\pm$ events. This effect has been estimated in simulation studying the difference in the interactions of protons and antiprotons with the detector material between $J/\psi(\to p\bar{p})K^\pm$ and $p\bar{p}K^\pm$ events generated uniformly over phase space. We obtained a m^2_{Kp}-dependent bias, up to 3% for the highest bin, for $A_{\rm raw}$.

To measure $A_{\rm raw}$ for charmonium modes, and in particular $J/\psi(\to p\bar{p})K^\pm$, a two-dimensional $(m_B, m_{p\bar{p}})$ simultaneous fit to the B^+ and B^- samples is performed. The systematic uncertainties are estimated by varying the fit functions and splitting the data sample according to trigger requirements or magnet polarities, and recombining the results from the subsamples. The procedure is applied to obtain a global value of A_{CP} as well as the variation of the asymmetry as a function of the Dalitz-plot variables. The results are $A_{CP} = -0.022 \pm 0.031({\rm stat}) \pm 0.007({\rm syst})$ for the full $p\bar{p}K^\pm$ spectrum, and $A_{CP} = -0.047 \pm 0.036({\rm stat}) \pm 0.007({\rm syst})$ for the region $m_{p\bar{p}} < 2.85\ {\rm GeV}/c^2$. Figure 7 shows the variation of A_{CP} as a function of the Dalitz-plot variables.

For the charmonium resonances, the values are $A_{CP}(\eta_c K^\pm) = 0.046 \pm 0.057({\rm stat}) \pm 0.007({\rm syst})$ and

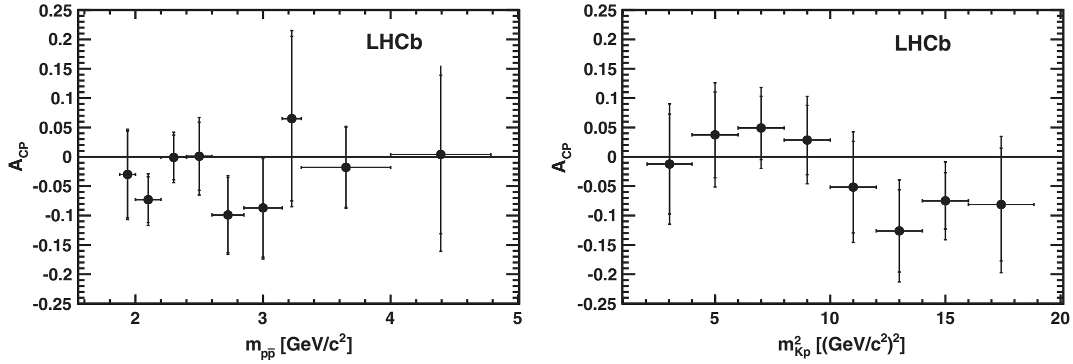

FIG. 7. Distribution of A_{CP} for the Dalitz-plot projections on $m_{p\bar{p}}$ and m^2_{Kp} for $B^\pm \to p\bar{p}K^\pm$ events. In the $m_{p\bar{p}}$ projection (left), the bin [2.85, 3.15] GeV/c^2 contains only the value of the charmless $p\bar{p}K^\pm$ after subtraction of the $\eta_c - J/\psi$ contribution. The m^2_{Kp} projection (right) has been obtained after removing the charmonia bands.

$A_{CP}(\psi(2S)K^\pm) = -0.002 \pm 0.123(\text{stat}) \pm 0.012(\text{syst})$. All results indicate no significant CP asymmetries.

VI. OBSERVATION OF THE $B^+ \to \bar{\Lambda}(1520)p$ DECAY

In the $p\bar{p}K^+$ spectrum, near the threshold of the neutral Kp combination, a peak in invariant mass at 1.52 GeV/c^2 is observed, as shown in Fig. 8, corresponding to the $\bar{u}\,\bar{d}\,\bar{s}$ resonance $\bar{\Lambda}(1520)$. The possible presence of higher $\bar{\Lambda}$ and $\bar{\Sigma}$ resonances may explain the enhancement in the range of [1.6, 1.7] GeV/c^2.

To identify the $\bar{\Lambda}(1520)$ signal, the B^+ signal is analyzed in the region $m_{Kp} \in [1.44, 1.585]$ GeV/c^2. Figure 9 shows the B signal weighted Kp invariant mass, and the expected $\bar{\Lambda}(1520)$ shape obtained from a model based on an asymmetric Breit-Wigner function derived from an EVTGEN [16] simulation of the decay $B^+ \to \bar{\Lambda}(1520)p$, convolved with a Gaussian resolution function, and a second-order polynomial function representing the tail of the non-$\bar{\Lambda}(1520)$ $B^+ \to p\bar{p}K^+$ decays.

These shapes are then used in a two-dimensional $(m_{p\bar{p}K^+}, m_{Kp})$ extended unbinned maximum likelihood fit to obtain the $B^+ \to \bar{\Lambda}(1520)p$ yield. The fit results in $N(B^+ \to \bar{\Lambda}(1520)p) = 47^{+12}_{-11}$ with a statistical significance of 5.3 standard deviations, obtained by comparing the likelihood at its maximum for the nominal fit and for the background-only hypothesis. Figure 10 shows the projections of the fit for the Kp and $p\bar{p}K^+$ invariant masses.

To test the robustness of the observation, different representations of the Kp background have been used, combining first- or second-order polynomials and a contribution modeled by a Breit-Wigner function, for which the mean (μ) and width (Γ) are allowed to vary within the known values of the $\Lambda(1600)$ baryon ($\mu \in [1.56, 1.7]$ GeV/c^2, $\Gamma \in [0.05, 0.25]$ GeV/c^2). Fits in a wider m_{Kp} range were also considered. In all cases the yield was stable with a statistical significance similar to the nominal fit case.

The branching fraction for the decay $B^+ \to \bar{\Lambda}(1520)p$ is derived from the ratio

$$\frac{\mathcal{B}(B^+ \to \bar{\Lambda}(1520)(\to K^+\bar{p})p)}{\mathcal{B}(B^+ \to J/\psi(\to p\bar{p})K^+)} = \frac{N_{\Lambda(1520)\to Kp}}{N_{J/\psi\to p\bar{p}}} \times \frac{\epsilon^{\text{gen}}_{J/\psi\to p\bar{p}}}{\epsilon^{\text{gen}}_{\Lambda(1520)\to Kp}} \times \frac{\epsilon^{\text{sel}}_{J/\psi\to p\bar{p}}}{\epsilon^{\text{sel}}_{\Lambda(1520)\to Kp}}, \quad (5)$$

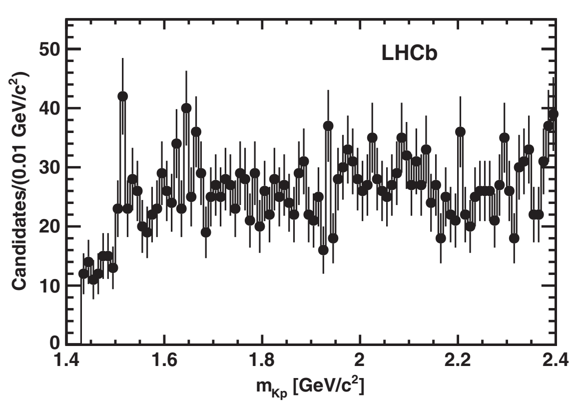

FIG. 8. Invariant mass m_{Kp} for the $B^+ \to p\bar{p}K^+$ candidates near threshold.

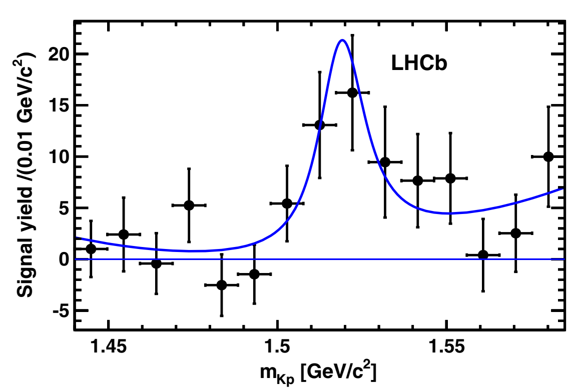

FIG. 9 (color online). Fit to the B signal weighted m_{Kp} distribution.

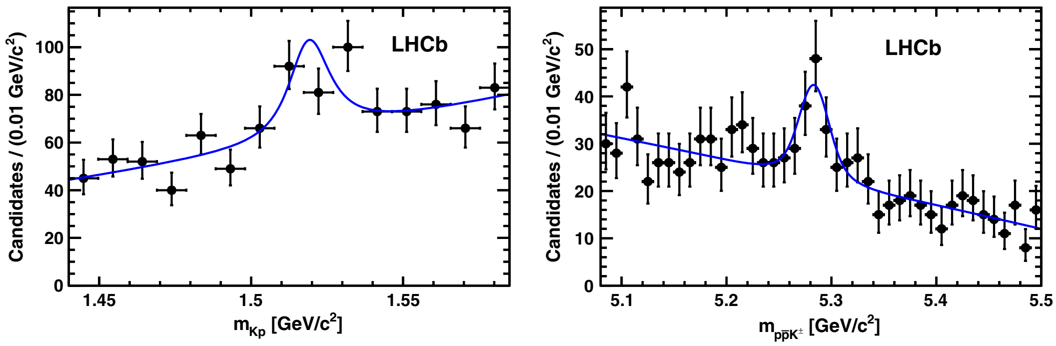

FIG. 10 (color online). Projections of (left) m_{Kp} and (right) $m_{p\bar{p}K^+}$ of the two-dimensional fit used to obtain the $B^+ \to \bar{\Lambda}(1520)p$ signal yield.

where N_i is the yield of the decay chain i, and $\epsilon^{\rm gen}$ denotes the efficiency after geometrical acceptance and simulation requirements. The global selection efficiency $\epsilon^{\rm sel}$ includes the reconstruction, the trigger, the offline selection, and the particle identification requirements. The ratio of branching fractions obtained is

$$\frac{\mathcal{B}(B^+ \to \bar{\Lambda}(1520)(\to K^+\bar{p})p)}{\mathcal{B}(B^+ \to J/\psi(\to p\bar{p})K^+)} = 0.041^{+0.011}_{-0.010}({\rm stat}) \pm 0.001({\rm syst}).$$

The systematic uncertainties include effects of the Kp background model, the particle identification, the limited simulation sample size, and the uncertainties on the relative trigger efficiencies, and they are summarized in Table VII. Convolving the systematic uncertainty with the statistical likelihood profile, the global significance is 5.1 standard deviations.

Using $\mathcal{B}(B^+ \to J/\psi K^+) = (1.016 \pm 0.033) \times 10^{-3}$, $\mathcal{B}(J/\psi \to p\bar{p}) = (2.17 \pm 0.07) \times 10^{-3}$ [26], and $\mathcal{B}(\Lambda(1520) \to K^-p) = 0.234 \pm 0.016$ [27], the branching fraction is

$$\mathcal{B}(B^+ \to \bar{\Lambda}(1520)p) = (3.9^{+1.0}_{-0.9}({\rm stat}) \pm 0.1({\rm syst}) \pm 0.3({\rm BF})) \times 10^{-7}.$$

The last error corresponds to the uncertainty on the secondary branching fractions. This result is in agreement with the upper limit set in Ref. [6], $\mathcal{B}(B^+ \to \bar{\Lambda}(1520)p) < 1.5 \times 10^{-6}$. Considering the separate $B^\pm$ signals in the range $m_{Kp} \in [1.44, 1.585]$ GeV$/c^2$, the yields are $N(B^-) = 50 \pm 12$ and $N(B^+) = 27 \pm 11$.

TABLE VII. Systematic uncertainties for the $\mathcal{B}(B^+ \to \bar{\Lambda}(1520)(\to K^+\bar{p})p)/\mathcal{B}(B^+ \to J/\psi(\to p\bar{p})K^+)$ branching fraction ratio. The total uncertainty is the sum in quadrature of the individual sources.

Source	Uncertainty (%)
Kp background	2.1
PID	1.7
Simulation sample size	0.5
Trigger	1.0
Total	2.9

VII. SUMMARY

Based on a data sample, corresponding to an integrated luminosity of 1.0 fb^{-1}, collected in 2011 by the LHCb experiment, an analysis of the three-body $B^+ \to p\bar{p}h^+$ decays ($h = K$ or π) has been performed. The dynamics of the decays has been probed using differential spectra of Dalitz-plot variables and signal-weighted Dalitz plots. The charmless $B^+ \to p\bar{p}K^+$ decay populates mainly the low $m^2_{p\bar{p}}$ and lower $m^2_{K^+\bar{p}}$-half regions whereas the $B^+ \to p\bar{p}\pi^+$ decay has a similar enhancement at low $m^2_{p\bar{p}}$ but with an upper $m^2_{\pi^+\bar{p}}$-half occupancy. From the occupation pattern of the Dalitz plots, it is likely that the $B^+ \to p\bar{p}K^+$ decay is primarily driven by $p\bar{p}$ rescattering with a secondary contribution from neutral Kp rescattering while the $B^+ \to p\bar{p}\pi^+$ decay is also dominated by $p\bar{p}$ rescattering but with a secondary contribution from doubly charged $(p\pi)^{++}$ rescattering, along the lines of the rescattering amplitude analysis performed in Ref. [28]. This difference of behavior is reflected in the values of the forward-backward asymmetry of the light meson in the $p\bar{p}$ rest frame

$$A_{\rm FB}(p\bar{p}K^+) = 0.370 \pm 0.018({\rm stat}) \pm 0.016({\rm syst}),$$
$$A_{\rm FB}(p\bar{p}\pi^+) = -0.392 \pm 0.117({\rm stat}) \pm 0.015({\rm syst}).$$

CP asymmetries for the $B^+ \to p\bar{p}K^+$ decay have been measured and no significant deviation from zero observed: $A_{CP} = -0.047 \pm 0.036({\rm stat}) \pm 0.007({\rm syst})$ for the charmless region $m_{p\bar{p}} < 2.85$ GeV$/c^2$, $A_{CP}(\eta_c K^\pm) = 0.046 \pm 0.057({\rm stat}) \pm 0.007({\rm syst})$ and $A_{CP}(\psi(2S)K^\pm) = -0.002 \pm 0.123({\rm stat}) \pm 0.012({\rm syst})$. These measurements are consistent with the current known values, $A_{CP}(B^\pm \to p\bar{p}K^\pm, m_{p\bar{p}} < 2.85\ {\rm GeV}/c^2) = -0.16 \pm 0.07$ [26], $A_{CP}(\eta_c K^\pm) = -0.16 \pm 0.08({\rm stat}) \pm 0.02({\rm syst})$ [8], and $A_{CP}(\psi(2S)K^{\pm}) = -0.025 \pm 0.024$ [26]. The absence of any significant charge asymmetry, contrary to the situation for $B^+ \to h^+h^+h^-$ decays [1,2], may be due to different long-range behavior. Final state interactions in the $B^+ \to p\bar{p}h^+$ case do not change the nature of the particles, such as $p\bar{p} \to p\bar{p}$ or $ph \to ph$, while $B^+ \to h^+h^+h^-$ modes can be affected by $\pi^+\pi^- \leftrightarrow K^+K^-$ scattering.

Finally, the observation of the decay $B^+ \to \bar{\Lambda}(1520)p$ is reported, with the branching fraction

$$\mathcal{B}(B^+ \to \bar{\Lambda}(1520)p) = (3.9^{+1.0}_{-0.9}(\text{stat}) \pm 0.1(\text{syst}) \pm 0.3(\text{BF})) \times 10^{-7}$$

in agreement with the current existing upper limit [6].

ACKNOWLEDGMENTS

We express our gratitude to our colleagues in the CERN accelerator departments for the excellent performance of the LHC. We thank the technical and administrative staff at the LHCb institutes. We acknowledge support from CERN and from the national agencies: CAPES, CNPq, FAPERJ and FINEP (Brazil); NSFC (China); CNRS/IN2P3 and Region Auvergne (France); BMBF, DFG, HGF and MPG (Germany); SFI (Ireland); INFN (Italy); FOM and NWO (The Netherlands); SCSR (Poland); MEN/IFA (Romania); MinES, Rosatom, RFBR and NRC "Kurchatov Institute" (Russia); MinECo, XuntaGal and GENCAT (Spain); SNSF and SER (Switzerland); NAS Ukraine (Ukraine); STFC (United Kingdom); NSF (USA). We also acknowledge the support received from the ERC under FP7. The Tier1 computing centers are supported by IN2P3 (France), KIT and BMBF (Germany), INFN (Italy), NWO and SURF (The Netherlands), PIC (Spain), GridPP (United Kingdom). We are thankful for the computing resources put at our disposal by Yandex LLC (Russia), as well as to the communities behind the multiple open source software packages that we depend on.

[1] R.Aaij *et al.*, LHCb Collaboration, Report No. LHCb-CONF-2012-028.
[2] R.Aaij *et al.*, LHCb Collaboration, Phys. Rev. Lett. **111**, 101801 (2013).
[3] R. Marshak, Riazuddin, and C. Ryan, *Theory of Weak Interactions in Particle Physics* (Wiley-Interscience, New York, NY, 1969).
[4] L. Wolfenstein, Phys. Rev. D **43**, 151 (1991).
[5] H. Y. Cheng, C. K. Chua, and A. Soni, Phys. Rev. D **71**, 014030 (2005).
[6] B. Aubert *et al.* (*BABAR* Collaboration), Phys. Rev. D **72**, 051101 (2005).
[7] B. Aubert *et al.* (*BABAR* Collaboration), Phys. Rev. D **76**, 092004 (2007).
[8] J.-T. Wei *et al.* (Belle Collaboration), Phys. Lett. B **659**, 80 (2008).
[9] R.Aaij *et al.*, LHCb Collaboration, Eur. Phys. J. C **73**, 2462 (2013).
[10] A. A. Alves, Jr. *et al.*, LHCb Collaboration, J. Inst. Electron. Commun. Eng. Jpn. **3**, S08005 (2008).
[11] M. Adinolfi *et al.*, Eur. Phys. J. C **73**, 2431 (2013).
[12] R. Aaij *et al.*, J. Inst. Electron. Commun. Eng. Jpn. **8**, P04022 (2013).
[13] V. V. Gligorov and M. Williams, J. Inst. Electron. Commun. Eng. Jpn. **8**, P02013 (2013).
[14] T. Sjöstrand, S. Mrenna, and P. Skands, J. High Energy Phys. 05 (2006) 026.
[15] I. Belyaev *et al.*, *Handling of the generation of primary events in Gauss, the LHCb simulation framework*, Nuclear Science Symposium Conference Record (NSS/MIC) (IEEE, Knoxville, TN, 2010), pp. 1155–1161.
[16] D. J. Lange, Nucl. Instrum. Methods Phys. Res., Sect. A **462**, 152 (2001).
[17] P. Golonka and Z. Was, Eur. Phys. J. C **45**, 97 (2006).
[18] J. Allison *et al.* (Geant4 Collaboration), IEEE Trans. Nucl. Sci. **53**, 270 (2006); S. Agostinelli *et al.* (Geant4 Collaboration), Nucl. Instrum. Methods Phys. Res., Sect. A **506**, 250 (2003).
[19] M. Clemencic, G. Corti, S Easo, C. R. Jones, S. Miglioranzi, M. Pappagallo, and P. Robbe, J. Phys. Conf. Ser. **331**, 032023 (2011).
[20] S. B. Athar *et al.* (CLEO Collaboration), Phys. Rev. D **73**, 032001 (2006).
[21] J. Z. Bai *et al.* (BES Collaboration), Phys. Rev. Lett. **91**, 022001 (2003).
[22] B. Aubert *et al.* (*BABAR* Collaboration), Phys. Rev. D **74**, 051101 (2006).
[23] J. Haidenbauer, U.-G. Meißner, and A. Sibirtsev, Phys. Rev. D **74**, 017501 (2006).
[24] H. Y. Cheng, Int. J. Mod. Phys. A **21**, 4209 (2006).
[25] M. Pivk and F. R. Le Diberder, Nucl. Instrum. Methods Phys. Res., Sect. A **555**, 356 (2005).
[26] J. Beringer *et al.* (Particle Data Group), Phys. Rev. D **86**, 010001 (2012).
[27] F. W. Wieland *et al.*, Eur. Phys. J. A **47**, 47 (2011); **47**, 133 (E) (2011).
[28] V. Laporta, Int. J. Mod. Phys. A **22**, 5401 (2007).

R. Aaij,[40] B. Adeva,[36] M. Adinolfi,[45] C. Adrover,[6] A. Affolder,[51] Z. Ajaltouni,[5] J. Albrecht,[9] F. Alessio,[37] M. Alexander,[50] S. Ali,[40] G. Alkhazov,[29] P. Alvarez Cartelle,[36] A. A. Alves, Jr.,[24,37] S. Amato,[2] S. Amerio,[21]

Y. Amhis,[7] L. Anderlini,[17,f] J. Anderson,[39] R. Andreassen,[56] J. E. Andrews,[57] R. B. Appleby,[53]
O. Aquines Gutierrez,[10] F. Archilli,[18] A. Artamonov,[34] M. Artuso,[58] E. Aslanides,[6] G. Auriemma,[24,m] M. Baalouch,[5]
S. Bachmann,[11] J. J. Back,[47] C. Baesso,[59] V. Balagura,[30] W. Baldini,[16] R. J. Barlow,[53] C. Barschel,[37] S. Barsuk,[7]
W. Barter,[46] Th. Bauer,[40] A. Bay,[38] J. Beddow,[50] F. Bedeschi,[22] I. Bediaga,[1] S. Belogurov,[30] K. Belous,[34]
I. Belyaev,[30] E. Ben-Haim,[8] G. Bencivenni,[18] S. Benson,[49] J. Benton,[45] A. Berezhnoy,[31] R. Bernet,[39] M.-O. Bettler,[46]
M. van Beuzekom,[40] A. Bien,[11] S. Bifani,[44] T. Bird,[53] A. Bizzeti,[17,h] P. M. Bjørnstad,[53] T. Blake,[37] F. Blanc,[38]
J. Blouw,[11] S. Blusk,[58] V. Bocci,[24] A. Bondar,[33] N. Bondar,[29] W. Bonivento,[15] S. Borghi,[53] A. Borgia,[58]
T. J. V. Bowcock,[51] E. Bowen,[39] C. Bozzi,[16] T. Brambach,[9] J. van den Brand,[41] J. Bressieux,[38] D. Brett,[53]
M. Britsch,[10] T. Britton,[58] N. H. Brook,[45] H. Brown,[51] I. Burducea,[28] A. Bursche,[39] G. Busetto,[21,q] J. Buytaert,[37]
S. Cadeddu,[15] O. Callot,[7] M. Calvi,[20,j] M. Calvo Gomez,[35,n] A. Camboni,[35] P. Campana,[18,37] D. Campora Perez,[37]
A. Carbone,[14,c] G. Carboni,[23,k] R. Cardinale,[19,i] A. Cardini,[15] H. Carranza-Mejia,[49] L. Carson,[52] K. Carvalho Akiba,[2]
G. Casse,[51] L. Castillo Garcia,[37] M. Cattaneo,[37] Ch. Cauet,[9] R. Cenci,[57] M. Charles,[54] Ph. Charpentier,[37] P. Chen,[3,38]
N. Chiapolini,[39] M. Chrzaszcz,[25] K. Ciba,[37] X. Cid Vidal,[37] G. Ciezarek,[52] P. E. L. Clarke,[49] M. Clemencic,[37]
H. V. Cliff,[46] J. Closier,[37] C. Coca,[28] V. Coco,[40] J. Cogan,[6] E. Cogneras,[5] P. Collins,[37] A. Comerma-Montells,[35]
A. Contu,[15,37] A. Cook,[45] M. Coombes,[45] S. Coquereau,[8] G. Corti,[37] B. Couturier,[37] G. A. Cowan,[49] D. C. Craik,[47]
S. Cunliffe,[52] R. Currie,[49] C. D'Ambrosio,[37] P. David,[8] P. N. Y. David,[40] A. Davis,[56] I. De Bonis,[4] K. De Bruyn,[40]
S. De Capua,[53] M. De Cian,[11] J. M. De Miranda,[1] L. De Paula,[2] W. De Silva,[56] P. De Simone,[18] D. Decamp,[4]
M. Deckenhoff,[9] L. Del Buono,[8] N. Déléage,[4] D. Derkach,[54] O. Deschamps,[5] F. Dettori,[41] A. Di Canto,[11]
H. Dijkstra,[37] M. Dogaru,[28] S. Donleavy,[51] F. Dordei,[11] A. Dosil Suárez,[36] D. Dossett,[47] A. Dovbnya,[42]
F. Dupertuis,[38] P. Durante,[37] R. Dzhelyadin,[34] A. Dziurda,[25] A. Dzyuba,[29] S. Easo,[48] U. Egede,[52] V. Egorychev,[30]
S. Eidelman,[33] D. van Eijk,[40] S. Eisenhardt,[49] U. Eitschberger,[9] R. Ekelhof,[9] L. Eklund,[50,37] I. El Rifai,[5]
Ch. Elsasser,[39] A. Falabella,[14,e] C. Färber,[11] G. Fardell,[49] C. Farinelli,[40] S. Farry,[51] D. Ferguson,[49]
V. Fernandez Albor,[36] F. Ferreira Rodrigues,[1] M. Ferro-Luzzi,[37] S. Filippov,[32] M. Fiore,[16] C. Fitzpatrick,[37]
M. Fontana,[10] F. Fontanelli,[19,i] R. Forty,[37] O. Francisco,[2] M. Frank,[37] C. Frei,[37] M. Frosini,[17,f] S. Furcas,[20]
E. Furfaro,[23,k] A. Gallas Torreira,[36] D. Galli,[14,c] M. Gandelman,[2] P. Gandini,[58] Y. Gao,[3] J. Garofoli,[58] P. Garosi,[53]
J. Garra Tico,[46] L. Garrido,[35] C. Gaspar,[37] R. Gauld,[54] E. Gersabeck,[11] M. Gersabeck,[53] T. Gershon,[47,37] Ph. Ghez,[4]
V. Gibson,[46] L. Giubega,[28] V. V. Gligorov,[37] C. Göbel,[59] D. Golubkov,[30] A. Golutvin,[52,30,37] A. Gomes,[2]
P. Gorbounov,[30,37] H. Gordon,[37] C. Gotti,[20] M. Grabalosa Gándara,[5] R. Graciani Diaz,[35] L. A. Granado Cardoso,[37]
E. Graugés,[35] G. Graziani,[17] A. Grecu,[28] E. Greening,[54] S. Gregson,[46] P. Griffith,[44] O. Grünberg,[60] B. Gui,[58]
E. Gushchin,[32] Yu. Guz,[34,37] T. Gys,[37] C. Hadjivasiliou,[58] G. Haefeli,[38] C. Haen,[37] S. C. Haines,[46] S. Hall,[52]
B. Hamilton,[57] T. Hampson,[45] S. Hansmann-Menzemer,[11] N. Harnew,[54] S. T. Harnew,[45] J. Harrison,[53]
T. Hartmann,[60] J. He,[37] T. Head,[37] V. Heijne,[40] K. Hennessy,[51] P. Henrard,[5] J. A. Hernando Morata,[36]
E. van Herwijnen,[37] A. Hicheur,[1] E. Hicks,[51] D. Hill,[54] M. Hoballah,[5] C. Hombach,[53] P. Hopchev,[4] W. Hulsbergen,[40]
P. Hunt,[54] T. Huse,[51] N. Hussain,[54] D. Hutchcroft,[51] D. Hynds,[50] V. Iakovenko,[43] M. Idzik,[26] P. Ilten,[12]
R. Jacobsson,[37] A. Jaeger,[11] E. Jans,[40] P. Jaton,[38] A. Jawahery,[57] F. Jing,[3] M. John,[54] D. Johnson,[54] C. R. Jones,[46]
C. Joram,[37] B. Jost,[37] M. Kaballo,[9] S. Kandybei,[42] W. Kanso,[6] M. Karacson,[37] T. M. Karbach,[37] I. R. Kenyon,[44]
T. Ketel,[41] A. Keune,[38] B. Khanji,[20] O. Kochebina,[7] I. Komarov,[38] R. F. Koopman,[41] P. Koppenburg,[40] M. Korolev,[31]
A. Kozlinskiy,[40] L. Kravchuk,[32] K. Kreplin,[11] M. Kreps,[47] G. Krocker,[11] P. Krokovny,[33] F. Kruse,[9]
M. Kucharczyk,[20,25,j] V. Kudryavtsev,[33] T. Kvaratskheliya,[30,37] V. N. La Thi,[38] D. Lacarrere,[37] G. Lafferty,[53]
A. Lai,[15] D. Lambert,[49] R. W. Lambert,[41] E. Lanciotti,[37] G. Lanfranchi,[18] C. Langenbruch,[37] T. Latham,[47]
C. Lazzeroni,[44] R. Le Gac,[6] J. van Leerdam,[40] J.-P. Lees,[4] R. Lefèvre,[5] A. Leflat,[31] J. Lefrançois,[7] S. Leo,[22]
O. Leroy,[6] T. Lesiak,[25] B. Leverington,[11] Y. Li,[3] L. Li Gioi,[5] M. Liles,[51] R. Lindner,[37] C. Linn,[11] B. Liu,[3] G. Liu,[37]
S. Lohn,[37] I. Longstaff,[50] J. H. Lopes,[2] N. Lopez-March,[38] H. Lu,[3] D. Lucchesi,[21,q] J. Luisier,[38] H. Luo,[49]
F. Machefert,[7] I. V. Machikhiliyan,[4,30] F. Maciuc,[28] O. Maev,[29,37] S. Malde,[54] G. Manca,[15,d] G. Mancinelli,[6]
J. Maratas,[5] U. Marconi,[14] P. Marino,[22,s] R. Märki,[38] J. Marks,[11] G. Martellotti,[24] A. Martens,[8] A. Martín Sánchez,[7]
M. Martinelli,[40] D. Martinez Santos,[41] D. Martins Tostes,[2] A. Martynov,[31] A. Massafferri,[1] R. Matev,[37] Z. Mathe,[37]
C. Matteuzzi,[20] E. Maurice,[6] A. Mazurov,[16,32,37,e] J. McCarthy,[44] A. McNab,[53] R. McNulty,[12] B. McSkelly,[51]
B. Meadows,[56,54] F. Meier,[9] M. Meissner,[11] M. Merk,[40] D. A. Milanes,[8] M.-N. Minard,[4] J. Molina Rodriguez,[59]
S. Monteil,[5] D. Moran,[53] P. Morawski,[25] A. Mordà,[6] M. J. Morello,[22,s] R. Mountain,[58] I. Mous,[40] F. Muheim,[49]
K. Müller,[39] R. Muresan,[28] B. Muryn,[26] B. Muster,[38] P. Naik,[45] T. Nakada,[38] R. Nandakumar,[48] I. Nasteva,[1]
M. Needham,[49] S. Neubert,[37] N. Neufeld,[37] A. D. Nguyen,[38] T. D. Nguyen,[38] C. Nguyen-Mau,[38,o] M. Nicol,[7]

V. Niess,[5] R. Niet,[9] N. Nikitin,[31] T. Nikodem,[11] A. Nomerotski,[54] A. Novoselov,[34] A. Oblakowska-Mucha,[26] V. Obraztsov,[34] S. Oggero,[40] S. Ogilvy,[50] O. Okhrimenko,[43] R. Oldeman,[15,d] M. Orlandea,[28] J. M. Otalora Goicochea,[2] P. Owen,[52] A. Oyanguren,[35] B. K. Pal,[58] A. Palano,[13,b] M. Palutan,[18] J. Panman,[37] A. Papanestis,[48] M. Pappagallo,[50] C. Parkes,[53] C. J. Parkinson,[52] G. Passaleva,[17] G. D. Patel,[51] M. Patel,[52] G. N. Patrick,[48] C. Patrignani,[19,i] C. Pavel-Nicorescu,[28] A. Pazos Alvarez,[36] A. Pellegrino,[40] G. Penso,[24,l] M. Pepe Altarelli,[37] S. Perazzini,[14,c] E. Perez Trigo,[36] A. Pérez-Calero Yzquierdo,[35] P. Perret,[5] M. Perrin-Terrin,[6] L. Pescatore,[44] E. Pesen,[61] K. Petridis,[52] A. Petrolini,[19,i] A. Phan,[58] E. Picatoste Olloqui,[35] B. Pietrzyk,[4] T. Pilař,[47] D. Pinci,[24] S. Playfer,[49] M. Plo Casasus,[36] F. Polci,[8] G. Polok,[25] A. Poluektov,[47,33] E. Polycarpo,[2] A. Popov,[34] D. Popov,[10] B. Popovici,[28] C. Potterat,[35] A. Powell,[54] J. Prisciandaro,[38] A. Pritchard,[51] C. Prouve,[7] V. Pugatch,[43] A. Puig Navarro,[38] G. Punzi,[22,r] W. Qian,[4] J. H. Rademacker,[45] B. Rakotomiaramanana,[38] M. S. Rangel,[2] I. Raniuk,[42] N. Rauschmayr,[37] G. Raven,[41] S. Redford,[54] M. M. Reid,[47] A. C. dos Reis,[1] S. Ricciardi,[48] A. Richards,[52] K. Rinnert,[51] V. Rives Molina,[35] D. A. Roa Romero,[5] P. Robbe,[7] D. A. Roberts,[57] E. Rodrigues,[53] P. Rodriguez Perez,[36] S. Roiser,[37] V. Romanovsky,[34] A. Romero Vidal,[36] J. Rouvinet,[38] T. Ruf,[37] F. Ruffini,[22] H. Ruiz,[35] P. Ruiz Valls,[35] G. Sabatino,[24,k] J. J. Saborido Silva,[36] N. Sagidova,[29] P. Sail,[50] B. Saitta,[15,d] V. Salustino Guimaraes,[2] B. Sanmartin Sedes,[36] M. Sannino,[19,i] R. Santacesaria,[24] C. Santamarina Rios,[36] E. Santovetti,[23,k] M. Sapunov,[6] A. Sarti,[18,l] C. Satriano,[24,m] A. Satta,[23] M. Savrie,[16,e] D. Savrina,[30,31] P. Schaack,[52] M. Schiller,[41] H. Schindler,[37] M. Schlupp,[9] M. Schmelling,[10] B. Schmidt,[37] O. Schneider,[38] A. Schopper,[37] M.-H. Schune,[7] R. Schwemmer,[37] B. Sciascia,[18] A. Sciubba,[24] M. Seco,[36] A. Semennikov,[30] K. Senderowska,[26] I. Sepp,[52] N. Serra,[39] J. Serrano,[6] P. Seyfert,[11] M. Shapkin,[34] I. Shapoval,[16,42] P. Shatalov,[30] Y. Shcheglov,[29] T. Shears,[51,37] L. Shekhtman,[33] O. Shevchenko,[42] V. Shevchenko,[30] A. Shires,[9] R. Silva Coutinho,[47] M. Sirendi,[46] N. Skidmore,[45] T. Skwarnicki,[58] N. A. Smith,[51] E. Smith,[54,48] J. Smith,[46] M. Smith,[53] M. D. Sokoloff,[56] F. J. P. Soler,[50] F. Soomro,[18] D. Souza,[45] B. Souza De Paula,[2] B. Spaan,[9] A. Sparkes,[49] P. Spradlin,[50] F. Stagni,[37] S. Stahl,[11] O. Steinkamp,[39] S. Stevenson,[54] S. Stoica,[28] S. Stone,[58] B. Storaci,[39] M. Straticiuc,[28] U. Straumann,[39] V. K. Subbiah,[37] L. Sun,[56] S. Swientek,[9] V. Syropoulos,[41] M. Szczekowski,[27] P. Szczypka,[38,37] T. Szumlak,[26] S. T'Jampens,[4] M. Teklishyn,[7] E. Teodorescu,[28] F. Teubert,[37] C. Thomas,[54] E. Thomas,[37] J. van Tilburg,[11] V. Tisserand,[4] M. Tobin,[38] S. Tolk,[41] D. Tonelli,[37] S. Topp-Joergensen,[54] N. Torr,[54] E. Tournefier,[4,52] S. Tourneur,[38] M. T. Tran,[38] M. Tresch,[39] A. Tsaregorodtsev,[6] P. Tsopelas,[40] N. Tuning,[40] M. Ubeda Garcia,[37] A. Ukleja,[27] D. Urner,[53] A. Ustyuzhanin,[52,p] U. Uwer,[11] V. Vagnoni,[14] G. Valenti,[14] A. Vallier,[7] M. Van Dijk,[45] R. Vazquez Gomez,[18] P. Vazquez Regueiro,[36] C. Vázquez Sierra,[36] S. Vecchi,[16] J. J. Velthuis,[45] M. Veltri,[17,g] G. Veneziano,[38] M. Vesterinen,[37] B. Viaud,[7] D. Vieira,[2] X. Vilasis-Cardona,[35,n] A. Vollhardt,[39] D. Volyanskyy,[10] D. Voong,[45] A. Vorobyev,[29] V. Vorobyev,[33] C. Voß,[60] H. Voss,[10] R. Waldi,[60] C. Wallace,[47] R. Wallace,[12] S. Wandernoth,[11] J. Wang,[58] D. R. Ward,[46] N. K. Watson,[44] A. D. Webber,[53] D. Websdale,[52] M. Whitehead,[47] J. Wicht,[37] J. Wiechczynski,[25] D. Wiedner,[11] L. Wiggers,[40] G. Wilkinson,[54] M. P. Williams,[47,48] M. Williams,[55] F. F. Wilson,[48] J. Wimberley,[57] J. Wishahi,[9] M. Witek,[25] S. A. Wotton,[46] S. Wright,[46] S. Wu,[3] K. Wyllie,[37] Y. Xie,[49,37] Z. Xing,[58] Z. Yang,[3] R. Young,[49] X. Yuan,[3] O. Yushchenko,[34] M. Zangoli,[14] M. Zavertyaev,[10,a] F. Zhang,[3] L. Zhang,[58] W. C. Zhang,[12] Y. Zhang,[3] A. Zhelezov,[11] A. Zhokhov,[30] L. Zhong,[3] and A. Zvyagin[37]

(LHCb Collaboration)

[1]*Centro Brasileiro de Pesquisas Físicas (CBPF), Rio de Janeiro, Brazil*
[2]*Universidade Federal do Rio de Janeiro (UFRJ), Rio de Janeiro, Brazil*
[3]*Center for High Energy Physics, Tsinghua University, Beijing, China*
[4]*LAPP, Université de Savoie, CNRS/IN2P3, Annecy-Le-Vieux, France*
[5]*Clermont Université, Université Blaise Pascal, CNRS/IN2P3, LPC, Clermont-Ferrand, France*
[6]*CPPM, Aix-Marseille Université, CNRS/IN2P3, Marseille, France*
[7]*LAL, Université Paris-Sud, CNRS/IN2P3, Orsay, France*
[8]*LPNHE, Université Pierre et Marie Curie, Université Paris Diderot, CNRS/IN2P3, Paris, France*
[9]*Fakultät Physik, Technische Universität Dortmund, Dortmund, Germany*
[10]*Max-Planck-Institut für Kernphysik (MPIK), Heidelberg, Germany*
[11]*Physikalisches Institut, Ruprecht-Karls-Universität Heidelberg, Heidelberg, Germany*
[12]*School of Physics, University College Dublin, Dublin, Ireland*
[13]*Sezione INFN di Bari, Bari, Italy*
[14]*Sezione INFN di Bologna, Bologna, Italy*

[15]*Sezione INFN di Cagliari, Cagliari, Italy*
[16]*Sezione INFN di Ferrara, Ferrara, Italy*
[17]*Sezione INFN di Firenze, Firenze, Italy*
[18]*Laboratori Nazionali dell'INFN di Frascati, Frascati, Italy*
[19]*Sezione INFN di Genova, Genova, Italy*
[20]*Sezione INFN di Milano Bicocca, Milano, Italy*
[21]*Sezione INFN di Padova, Padova, Italy*
[22]*Sezione INFN di Pisa, Pisa, Italy*
[23]*Sezione INFN di Roma Tor Vergata, Roma, Italy*
[24]*Sezione INFN di Roma La Sapienza, Roma, Italy*
[25]*Henryk Niewodniczanski Institute of Nuclear Physics Polish Academy of Sciences, Kraków, Poland*
[26]*Faculty of Physics and Applied Computer Science, AGH-University of Science and Technology, Kraków, Poland*
[27]*National Center for Nuclear Research (NCBJ), Warsaw, Poland*
[28]*Horia Hulubei National Institute of Physics and Nuclear Engineering, Bucharest-Magurele, Romania*
[29]*Petersburg Nuclear Physics Institute (PNPI), Gatchina, Russia*
[30]*Institute of Theoretical and Experimental Physics (ITEP), Moscow, Russia*
[31]*Institute of Nuclear Physics, Moscow State University (SINP MSU), Moscow, Russia*
[32]*Institute for Nuclear Research of the Russian Academy of Sciences (INR RAN), Moscow, Russia*
[33]*Budker Institute of Nuclear Physics (SB RAS) and Novosibirsk State University, Novosibirsk, Russia*
[34]*Institute for High Energy Physics (IHEP), Protvino, Russia*
[35]*Universitat de Barcelona, Barcelona, Spain*
[36]*Universidad de Santiago de Compostela, Santiago de Compostela, Spain*
[37]*European Organization for Nuclear Research (CERN), Geneva, Switzerland*
[38]*Ecole Polytechnique Fédérale de Lausanne (EPFL), Lausanne, Switzerland*
[39]*Physik-Institut, Universität Zürich, Zürich, Switzerland*
[40]*Nikhef National Institute for Subatomic Physics, Amsterdam, The Netherlands*
[41]*Nikhef National Institute for Subatomic Physics and VU University Amsterdam, Amsterdam, The Netherlands*
[42]*NSC Kharkiv Institute of Physics and Technology (NSC KIPT), Kharkiv, Ukraine*
[43]*Institute for Nuclear Research of the National Academy of Sciences (KINR), Kyiv, Ukraine*
[44]*University of Birmingham, Birmingham, United Kingdom*
[45]*H.H. Wills Physics Laboratory, University of Bristol, Bristol, United Kingdom*
[46]*Cavendish Laboratory, University of Cambridge, Cambridge, United Kingdom*
[47]*Department of Physics, University of Warwick, Coventry, United Kingdom*
[48]*STFC Rutherford Appleton Laboratory, Didcot, United Kingdom*
[49]*School of Physics and Astronomy, University of Edinburgh, Edinburgh, United Kingdom*
[50]*School of Physics and Astronomy, University of Glasgow, Glasgow, United Kingdom*
[51]*Oliver Lodge Laboratory, University of Liverpool, Liverpool, United Kingdom*
[52]*Imperial College London, London, United Kingdom*
[53]*School of Physics and Astronomy, University of Manchester, Manchester, United Kingdom*
[54]*Department of Physics, University of Oxford, Oxford, United Kingdom*
[55]*Massachusetts Institute of Technology, Cambridge, Massachusetts, USA*
[56]*University of Cincinnati, Cincinnati, Ohio, USA*
[57]*University of Maryland, College Park, Maryland, USA*
[58]*Syracuse University, Syracuse, New York, USA*
[59]*Pontifícia Universidade Católica do Rio de Janeiro (PUC-Rio), Rio de Janeiro, Brazil associated to Universidade Federal do Rio de Janeiro (UFRJ), Rio de Janeiro, Brazil*
[60]*Institut für Physik, Universität Rostock, Rostock, Germany associated to Physikalisches Institut, Ruprecht-Karls-Universität Heidelberg, Heidelberg, Germany*
[61]*Celal Bayar University, Manisa, Turkey associated to European Organization for Nuclear Research (CERN), Geneva, Switzerland*

[a]Also at Università di Firenze, Firenze, Italy.
[b]Also at Università della Basilicata, Potenza, Italy.
[c]Also at Università di Modena e Reggio Emilia, Modena, Italy.
[d]Also at Università di Padova, Padova, Italy.
[e]Also at Università di Milano Bicocca, Milano, Italy.
[f]Also at LIFAELS, La Salle, Universitat Ramon Llull, Barcelona, Spain.
[g]Also at Università di Bologna, Bologna, Italy.
[h]Also at Università di Roma Tor Vergata, Roma, Italy.
[i]Also at Università di Genova, Genova, Italy.

[j]Also at Università di Ferrara, Ferrara, Italy.
[k]Also at Università di Cagliari, Cagliari, Italy.
[l]Also at Scuola Normale Superiore, Pisa, Italy.
[m]Also at Hanoi University of Science, Hanoi, Viet Nam.
[n]Also at Università di Bari, Bari, Italy.
[o]Also at Università di Roma La Sapienza, Roma, Italy.
[p]Also at Università di Pisa, Pisa, Italy.
[q]Also at Institute of Physics and Technology, Moscow, Russia.
[r]Also at Università di Urbino, Urbino, Italy.
[s]Also at P.N. Lebedev Physical Institute, Russian Academy of Science (LPI RAS), Moscow, Russia.